

Meta-plasticity and memory in multi-level recurrent feed-forward networks

Gianmarco Zanardi,^{1,2} Paolo Bettotti,¹ Jules Morand,^{1,2} Lorenzo Pavesi,¹ and Luca Tubiana^{1,2,*}

¹*Physics Department, University of Trento, via Sommarive, 14 I-38123 Trento (IT)*

²*INFN-TIFPA, Trento Institute for Fundamental Physics and Applications, I-38123 Trento (IT)*

Network systems can exhibit memory effects in which the interactions between different pairs of nodes adapt in time, leading to the emergence of preferred connections, patterns, and sub-networks. To a first approximation, this memory can be modelled through a “plastic” Hebbian or homophily mechanism, in which edges get reinforced proportionally to the amount of information flowing through them. However, recent studies on glia-neuron networks have highlighted how memory can evolve due to more complex dynamics, including multi-level network structures and “meta-plastic” effects that modulate reinforcement. Inspired by those systems, here we develop a simple and general model for the dynamics of an adaptive network with an additional meta-plastic mechanism that varies the rate of Hebbian strengthening of its edge connections. Specifically, we consider a biased random walk on a cyclic feed-forward network. The random walk chooses its steps according to the weights of the network edges. The weights evolve through a Hebbian mechanism modulated by a meta-plastic reinforcement, biasing the walker to prefer edges that have been already explored. We study the dynamical emergence (memorization) of preferred paths and their retrieval and identify three regimes: one dominated by the Hebbian term, one in which the meta-reinforcement drives memory formation, and a balanced one. We show that, in the latter two regimes, meta-reinforcement allows for the retrieval of a previously stored path even after weights have been reset to zero to erase Hebbian memory.

I. INTRODUCTION

Several biological, ecological and social systems, such as for example internet communities, human populations, epigenetic interactions, and ecosystems, can be described as networks of interacting agents [1–8]. These networks are in general adaptive: their topology and the strength of their connections evolve in time in response to the interaction between the agents. This gives rise to the emergence of transitions and collective behaviours, e.g. network polarisation and opinion dynamics [9–11], epidemic spreading [12–14] or mobility and diffusion patterns [15, 16].

Network dynamics often display memory effects, where a preference for certain connections or paths emerges over time as a result of interactions amongst the agents or external effects: this is the case for example of echo chambers in social network [11, 17, 18], preferred patterns mobility networks [16, 19] and, of course, memories in the brain [20–22].

The brain provides a remarkable example of adaptive and memorising network, with multiple forms of memory across different time-scales [23, 24]. Neurons can be considered agents connected by synapses that exchange neurotransmitter molecules to communicate. The variation in strength of specific synapses, called *plasticity*, leads to the formation of patterns of neurons that activate together, which are assumed to

encode our memories [25–28], as modelled by Hopfield [20, 21].

The first notable theoretical framework of plasticity was presented by Hebb [26]: summarised with the famous sentence «neurons that fire together wire together». Hebbian theory states that when two neurons repeatedly activate together their synapses become stronger, making it easier to happen again in the future. This very fundamental description of plastic synapses provides the basis for numerous more advanced memory models [29–32]. In this context, the susceptibility of a synapse to the activity of the neurons it connects is called *learning rate*: the higher the rate, the greater the strengthening of the synapse when a signal traverses it.

Analogous concepts to plasticity exist for adaptive networks other than the brain, e.g. homophily bonding [33, 34], mutualistic/antagonistic interactions [35] and prey/predator dynamics [36] in social, economic or ecological networks respectively. These concepts provide the bases for emergent network properties and introduce non-Markovianity in the dynamics, effectively introducing a memory kernel for the process [16, 37, 38].

In the last two decades, it has also become increasingly clear that plasticity in the brain is further modulated by glial cells, particularly astrocytes, that interact chemically with synapses [39–42] over time-scales that can be larger compared to the intrinsic ones of neurons [43]. The interaction between glial cells and neurons has been described either in terms of tripartite synapses, or of “multiplex” networks [44], i.e. networks composed of two levels: the neuronal one and the glial

* Corresponding author: luca.tubiana@unitn.it

one, which constitute two sub-networks interacting with each other. Multi-level structures such as the glial-neuron system can also be found in other systems, such as interconnected social networks, ecological networks or bio-physical and bio-molecular networks [44–48].

One possible effect of the interaction between glial cells and neurons is to vary the rate of synaptic reinforcement modifying their learning rate. This *meta-plastic* reinforcement has been studied in theoretical models [49, 50]. In particular, Fusi *et al.* [49] employed a mean-field approach to study how the inclusion of meta-plasticity in a model of binary synapses helps preserve memory in terms of signal-to-noise ratio. Arguably, similar dynamics should act in other kind of network systems, for example in social networks by priming the susceptibility of agents to information coming from trusted connections.

The interplay between plastic and meta-plastic reinforcement (which we simply call “reinforcement” and “meta-reinforcement”) in a multi-level network is the subject of the present study, which focuses on the dynamical creation and retrieval of a memorised pattern. Specifically, we consider an idealised system constituted by a recurrent, feed-forward adaptive network that is traversed by a random walk (RW) and investigate how it can memorise and retrieve a pattern through the RW dynamics. If the nodes are interpreted as agents, the RW process models the communication between them; if they are interpreted as locations, the RW process models an active agent moving between different places. In both cases the memorisation and retrieval happen by changing the weights of the connections between different nodes so that the RW is biased to choose paths that it has already explored: the memory is stored in the network itself.

Biased RWs provide a standard model to investigate the mathematical properties of non-Markovian systems, for example their limit behaviours and phases [51–55], including proofs of the walker being asymptotically confined to an attractor [56–59]. To enable analytical treatment, such models feature particularly simple non-Markovian dynamics, like exponential or power-law reinforcement equations, resulting in weights that grow indefinitely and limiting their applicability to biophysical systems.

In our model, the weights of edges in the network grow according to a sigmoid function when the walker traverses them, resulting in a Hebbian reinforcement term that is asymptotically bounded by an upper value. Meta-reinforcement increases the learning rate of the Hebbian dynamics and is stochastically distributed between edges pertaining to local groups: this adds a second layer

to the network, inducing a local coordination between nodes. These assumptions reflect the presence of undefined interactions or unknown driving factors in the phenomena to model, e.g. an unknown molecular mechanisms in astrocytes in a neuron-glia network or undetected, possibly off-line verbal communications between people in a social network. Following these scenarios, we further assume that reinforcements acts on a fast time-scale, and meta-reinforcement on a slower one. Due to the complexity of our dynamics, we conduct our work mostly through numerical simulations.

Our results show that the addition of a second memorising component improves the capabilities of the model beyond those of regular reinforcement. In particular, we obtain three regimes in the space of parameters, characterised by one component of the dynamics imposing itself on the others and controlling the outcome of the RW process. In one of these regimes, second-order adaptation is capable of driving the RW while reinforcement alone is ineffective; moreover it allows for proper retrieval of the memorised path even after the Hebbian memory is completely erased.

The manuscript is organised as follows. In Sec. II, we define the model. We describe the relevant observables, path entropy and path distance, in Sec. III. In Sec. IV, we present the results of our simulations in terms of the formation of a memory engram and of its retrieval afterwards, testing various combinations of values for the parameters of our model. Finally, in Sec. V we analyse an asymptotic regime of the model and show how this can clarify some of the results obtained in Sec. IV.

II. THE MODEL

A. Network structure

In this work we consider a *cyclic feed-forward network* (CFFN). This choice simplifies calculations while preserving the rich interplay between the two memory dynamics of the process. As is standard for feed-forward networks, our network is divided in L layers, labelled $\ell \in \{1, \dots, L\}$, of N nodes each, see Fig. 1. Each node in layer ℓ is connected to all nodes of layer $\ell + 1$, those of layer $\ell = L$ are connected to those of layer $\ell = 1$, ensuring that the network has a recurrent structure (*cyclic*). All edges are directed from layer ℓ towards layer $\ell + 1$. The walker can only traverse them in this direction (*feed-forward*). Fig. 1a) depicts the resulting network topology. The specific CFFN we employ for the simulations presented in Sec. IV is composed of $L = 20$ layers of $N = 10$ nodes each. While this size has been chosen for nu-

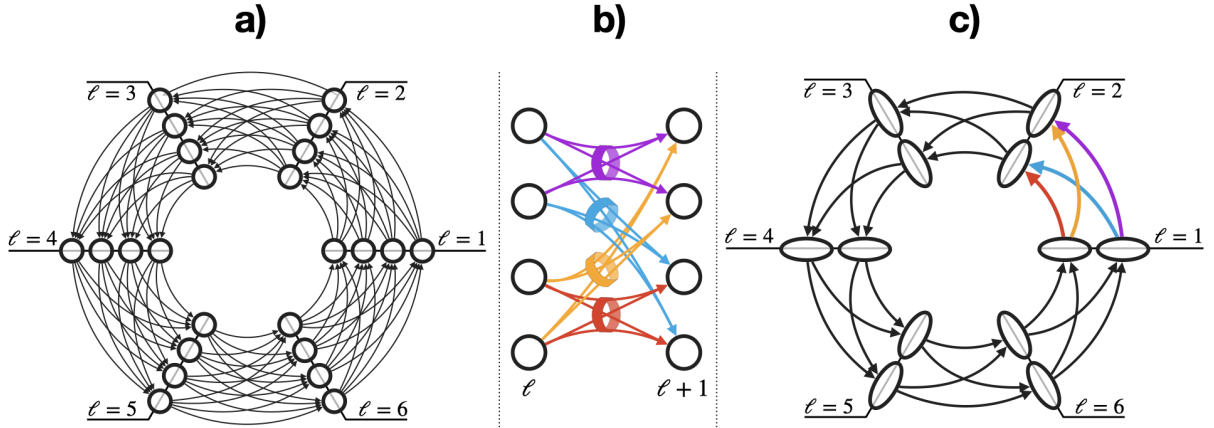


Figure 1. a) Example of cyclic feed-forward network with 6 layers, labelled by ℓ , with 4 nodes each. b) The grouping of the edges, between consecutive layers of the network in panel a), into a partition of 4 edge groups (represented by the 4 colours), accordingly with our chosen rule (see main text); edges are distorted to ease visualisation of the grouping. c) The resulting network after edge grouping yields a lower resolution (coarse-grained) network analogous (self-similar) to that in panel a); edge colours between layers $\ell = 1$ and $\ell = 2$ refer to the edge groups of panel b).

merical convenience changing the number of layers or that of nodes does not modify the qualitative behaviour discussed in the rest of this manuscript.

To implement plasticity, the edges of the network are weighted proportionally to the number of times the walker has crossed them in the recent past. We refer to this property as *frecency* (a blend of frequency and recency) and through it we implement an Hebbian rule to bias the future movements of the walker, as described in Subsec. II B.

To model a meta-plastic behaviour on a longer time-scale and across different nearby edges, we enrich the network with a second level of coordination between local groups of edges, which can be seen as a second system interacting with the CFFN. First, we cluster the nodes in each layer ℓ in pairs, obtaining $\frac{N}{2}$ pairs per layer. Each pair corresponds to a coarse-grained (CG) node. Then, we consider the four edges going from the two nodes of a pair in layer ℓ to the two of a pair in layer $\ell + 1$: these four edges constitute one edge group and share the meta-reinforcement contribution between them, proportionally to the weight of each one. The grouping procedure is illustrated in Fig. 1b). By construction, between each layer of nodes we get $\frac{N^2}{4}$ groups of 4 edges each, and each edge belongs to one and only one group. This choice ensures that meta-reinforcement only acts locally, i.e., between edges connecting neighbouring nodes, and effectively coarse-grains the entire network, as shown in Fig. 1c).

B. Reinforcement dynamics

To recover Hebbian-type memory dynamics, we employ an edge-reinforced random walk (ERRW) [60] and adapt it so that the memory can degrade, producing an effective short-term memory (STM) as explained below.

For a generic random walk on a network, the probability $p(i \rightarrow j)$ to go from node i to node j is given by the weight w^ε of the edge $\varepsilon = i \rightarrow j$ connecting the two nodes, normalised over all edges leaving i :

$$p(\varepsilon) = p(i \rightarrow j) = \frac{w^\varepsilon}{\sum_{\varepsilon' \in k^+(i)} w^{\varepsilon'}}, \quad (1)$$

where $k^+(i)$ is the set of all out-going edges of node i . In an ERRW, each edge weight is time-dependent: it is increased (reinforced) each time the walker passes through it, and all edge weights decay over the same characteristic time-scale, see Eq.s (2) - (3). The network becomes adaptive.

To be compatible with any real and finite system, we bound the maximum value of the weights. To do so, we consider each weight w_t^ε to be given by a sigmoid function $\sigma(s_t^\varepsilon)$ of the *frecency* of traversals s_t^ε . This quantity takes into account the frequency of recent traversals of an edge and evolves according to Eq. 2:

$$s_{t+1}^\varepsilon = s_t^\varepsilon e^{-\frac{1}{\tau'}} + \mathbb{I}[\eta_t = \varepsilon]. \quad (2)$$

The first term on the RHS of Eq. 2 causes the decay of s_t^ε with characteristic time τ' irrespective of the edge, η_t , traversed by the walker at time-

step t . The second term $\mathbb{I}[\eta_t = \varepsilon]$ yields 1 if $\varepsilon = \eta_t$ and 0 otherwise: it increments by 1 the frequency of the edge crossed at time-step t . We take s_t^ε to be defined on \mathbb{R}^+ and we set $s_0^\varepsilon = 0$ for all edges at time $t = 0$.

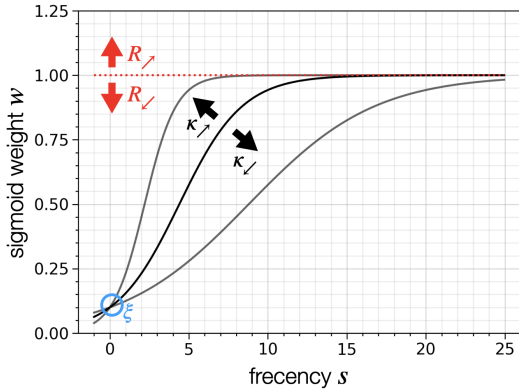


Figure 2. Examples of the dynamic on logistic functions $\sigma(s)$ versus frequency (black curves) for the regularised growth of edge weights, see Eq. 3, and the role of the parameters involved: ξ ensures that in $s = 0$ all functions have the same initial value regardless of the other parameters (see the blue circle). R sets the upper asymptote for the function (red dotted line): lowering R ($R_{<}$) shrinks the function while increasing it ($R_{>}$) stretches the function. Finally, κ controls how rapidly the function approaches its asymptotes, hence lowering κ ($\kappa_{<}$) flattens the function while increasing it ($\kappa_{>}$) makes the function steeper. More detailed explanations about the function and parameters can be found in the text.

The model does not depend on the specific sigmoid function σ adopted. For simplicity, we choose to use of the logistic function:

$$w_t^\varepsilon = \sigma(s_t^\varepsilon) = \frac{R}{1 + \exp(-\kappa s_t^\varepsilon + \xi)}, \quad (3)$$

which is analogous to the Hill equation, employed in bio-chemistry to describe ligands binding as a function of their concentration [61]. Parameters ξ , R , and κ in Eq. (3) set respectively the minimum and maximum values of the weight, and the steepness of the curve. Their roles are reported graphically in Fig. 2. We set $\xi = \ln(NR - 1)$, such that the initial value of weights is always $w_0 = R/(1+e^\xi) = 1/N$ ¹.

For ease of interpretation, in the following we adopt the quantity $p_{as}(R)$, representing the maximum probability for an edge to be traversed by a walker. This corresponds to the case in which the

walker has chosen the same edge for $n \rightarrow \infty$ steps, so that its weight is $w_{as} = R$, while all other edges leaving that node have weight w_0 :

$$p_{as} = \frac{w_{as}}{w_{as} + w_0(N-1)} = \frac{R}{R + \frac{N-1}{N}}. \quad (4)$$

p_{as} is never reached as in general, all weights $w_t > w_0 \forall t > 0$, and s_t cannot increase indefinitely, as explained in detail in Sec. V.

Together, equations (1) – (3) describe an ERRW able to memorise how frequently each edge of the network was traversed in a near past. This implements a STM, characterised by two independent time-scales: κ , in units of $\frac{1}{s}$, which sets the learning rate for the weight reinforcement, and τ' , in units of $\Delta t = 1$, for the decay time of s itself, which leads to the decay of the weight to its base-value $w(0) = \frac{1}{N}$.

We highlight here that in a cyclic network one can measure time both in units of time-step $\Delta t = 1$, reflecting the steps η of the walker, or in units of loops $\mathcal{L} = L * \Delta t$, or cycles, around the network. The first choice simplifies slightly the equations, while the second facilitates the analysis and makes it independent of the number of layers in the network. For these reasons in the results we measure time in units of \mathcal{L} and the characteristic decay time of the STM as $\tau = \frac{\tau'}{L}$.

C. Meta-reinforcement

The second memory dynamics acts directly on the learning-rate κ of the edges, making some connections more apt to be reinforced than others and thus facilitating their reinforcement. As explained before, this mimics a memory acting on long time-scales, without decay, and shared between neighbouring connections in a group. No other details are considered, so the dynamics is assumed to be stochastic. This “meta-reinforcement” dynamics is also bounded by a sigmoid $\sigma^{(\kappa)}$ (defined explicitly in Eq. (7)). The learning rate κ^ε evolves as follows:

$$\kappa_t^\varepsilon = \kappa_0 + \sigma^{(\kappa)}(y_t^\varepsilon) \quad (5)$$

where κ_0 is the initial learning rate and y_t^ε is a monotonically growing stochastic variable that models the random activation at time-step t of the edge-group, \mathcal{G} , to which edge ε_t belongs, see Sec. II A.

The variable y^ε driving the time evolution of κ is updated at each step according to a stochastic contribution that is split amongst the active edges

¹ Note that a change in the number of nodes in the network would reflect in a change of w_0

within \mathcal{G} according to their weights:

$$y_{t+1}^\varepsilon = y_t^\varepsilon + c \frac{w_t^\varepsilon}{\sum_{\varepsilon' \in \mathcal{G}} w_t^{\varepsilon'}} \Theta(w_t^\varepsilon - w_{min}) \chi_t^\mathcal{G}, \quad (6)$$

where Θ is the Heavyside theta function, $c \geq 0$ controls the rate of meta-reinforcement, and $\chi_t^\mathcal{G} \sim \mathcal{B}(p_{mr})$ is a stochastic variable following a Bernoulli process: $\chi_t^\mathcal{G} \sim \mathcal{B}(p_{mr})$ gives 1 with probability p_{mr} and 0 otherwise. We define the active edges as those for which $w_t^\varepsilon \geq w_{min}$. Note that while edges that are not active are not able to experience the meta-reinforcement contribution, they are still counted in the denominator. Finally, we set $w_{min} = w \left(s = e^{-\frac{s}{\tau}} \right)$ so that edges that have not been traversed during the last 5 loops are ignored.

The $\sigma^{(\kappa)}$ function of Eq. (5) is an edge-independent shifted logistic function with constant parameters:

$$\sigma^{(\kappa)}(y) = \frac{2.5}{1 + \exp(-y)} - 1.25. \quad (7)$$

This form ensures that $\sigma^{(\kappa)}(0) = 0$ and $\sigma^{(\kappa)}(\infty) = 1.25$, so that $\kappa_t^\varepsilon \leq 2.25$ given $\kappa_0 = 1$. Furthermore, the -1.25 shift makes meta-reinforcement most responsive for small values of y^2 . Finally, we normalise the steepness of $\sigma^{(\kappa)}$ to 1 for simplicity.

Through Eq.s (5) – (6), the meta-reinforcement dynamics adds a long-term memory built on top of the STM introduced in Sec. II B. This memory form never fades: it is unaffected by the decay in frequency from Eq. (2) and we do not consider any decay mechanism for y in Eq. (6) as we are assuming that it would happen over a much larger time-scale compared to any other involved in the model and can hence be neglected. The time-scale for the meta-reinforcement dynamics is controlled by both the meta-reinforcement coefficient c and the probability p_{mr} for the stochastic variable in Eq. (6). Having the contribution per unit time-step be split amongst four edges, proportionally to the relative weights, further slows the dynamics and hence increases its time-scale. Moreover, this dynamics is a second-order reinforcement and hence its effect on the RW can take longer to manifest, meaning its “effective” time-scale is even greater.

III. OBSERVABLES

We analyse the capability of the system to memorise through two quantities: a) a Shannon path entropy, or “caliber” [62], which captures the degree of equi-probability of the system, and b) a layer-wise distance between different paths. Both are defined as functions of time, measured in loops \mathcal{L} on the CFFN, to describe memory as it emerges.

A. Shannon path entropy

Path entropy, often referred to as “caliber” [62], is a Shannon entropy functional over the possible trajectories of a dynamical system, which in our case are the possible paths $\{\Gamma\}$ that can be taken by the random walker after loop \mathcal{L} :

$$S_{\mathcal{L}} = - \sum_{\{\Gamma\}} p_{\mathcal{L}}(\Gamma) \ln(p_{\mathcal{L}}(\Gamma)), \quad (8)$$

where $p_{\mathcal{L}}(\Gamma)$ is the probability of the walker taking path Γ according to the state of the network in loop \mathcal{L} . Analogously to Shannon entropy, path entropy is maximal when the system is in a condition of equi-probability, and minimal when just one specific path has been memorised and is constantly traversed. Since the weights of the network get updated at each step, $S_{\mathcal{L}}$ allows to measure how much the system is memorising as a function of time.

To compute $S_{\mathcal{L}}$ we leverage the CFFN structure. This allows us to define transfer matrices from one layer to the next based on the weights of the edges at loop \mathcal{L} . $T_{\mathcal{L}}^{\ell \leftarrow \ell-1}$ is the $N \times N$ matrix describing the probability to go from each individual node in layer $\ell - 1$ to each in layer ℓ during loop \mathcal{L} . To get the probability of paths involving more layers, one simply multiplies the corresponding sequence of matrices. Finally, in a CFFN the starting point of a loop is the end of the previous one, therefore $n_{(\mathcal{L})}^{\ell=0} \equiv n_{(\mathcal{L}-1)}^{\ell=L}$. Hence, $p_{\mathcal{L}}(n^{\ell=0})$ is the probability for the previous loop to end in node $n_{\mathcal{L}}^{\ell=0}$ and $T_{\mathcal{L}}^{\ell=1 \leftarrow \ell-1=0}$ is the transition matrix from the last layer of the previous loop to the first of the current loop. In this formalism, the entropy of the RW at loop \mathcal{L} is explicitly given by Eq. (9). The mathematical derivation is reported in Supplementary Material.

² Because the sigmoid function is most responsive in its centre, where its first-order derivative is the highest, this

requirement can be expressed through the second-order derivative as $\left. \frac{\partial^2}{\partial y^2} \sigma^{(\kappa)} \right|_{y=0} = 0$.

$$S_{\Sigma} = - \sum_{\{\Gamma\}} \left[\prod_{\ell=1}^L p_{\Sigma}(n^{\ell=0}) T_{\Sigma}^{\ell \leftarrow \ell - 1} \right] \left[\ln(p_{\Sigma}(n^{\ell=0})) + \sum_{\ell=1}^L \ln(T_{\Sigma}^{\ell \leftarrow \ell - 1}) \right]. \quad (9)$$

To remove any dependence on the size of the CFFN, we normalise the entropy of Eq. (9) w.r.t. its value at equi-probability.

B. Distance between paths

To further analyse our results we need to compare the distance between a path, i.e. a sequence of nodes $\Gamma = (n^{\ell=1}, \dots, n^{\ell=L})$ and a meta-reinforced, CG path, i.e. a sequence of CG nodes $\Gamma_{CG} = (\{n\}_{CG}^{\ell=1}, \dots, \{n\}_{CG}^{\ell=L})$, where $\{n\}_{CG}^{\ell}$ represents a set of nodes corresponding to one of the CG nodes depicted in Fig. 1c). Leveraging the CFFN structure of our network, this distance can be defined through a Hamming distance that counts the layers in which the node of path Γ is included in the CG node of Γ_{CG} . Mathematically, it is computed as

$$d(\Gamma, \Gamma_{CG}) = 1 - \frac{1}{L} \sum_{\ell=1}^L \mathbb{I}[n^{\ell} \in \{n\}_{CG}^{\ell}]. \quad (10)$$

We note that with this definition one can also define a distance between two paths Γ_1 and Γ_2 , with respect to a given CG path Γ_{CG}

$$d(\Gamma_1, \Gamma_2) = d(\Gamma_1, \Gamma_{CG}) + d(\Gamma_2, \Gamma_{CG}). \quad (11)$$

While path distances are intrinsically noisier compared to the Shannon path entropy, the two quantities are complementary. The latter gives us a measure of the memorisation of the system, while the former can be used to measure how precisely a given path has been memorised.

IV. NUMERICAL RESULTS

We perform numerical simulations of a biased random walker on a CFFN, as described in sec. II. To characterise the interplay between reinforcement and meta-reinforcement, we consider an idealised case in which only one set of group edges Γ_{CG} gets meta-reinforced as shown in Fig. 3a). We identify Γ_{CG} with the set of consecutive edge nodes that contains the path chosen by the walker during the first loop, Γ_1 . Thus, Γ_{CG} identifies a coarse-grained version of Γ_1 passing through two adjacent nodes on each layer. We use Γ_{CG} as a reference path to evaluate whether the system is able to memorise and retrieve a given path under dif-

ferent conditions, described below. For simplicity, we force Γ_{CG} and hence Γ_1 to be a closed path.

The simulations are structured so that the dynamics goes through three stages. For the first T_1 loops the system follows a normal Hebbian dynamics, without meta-reinforcement. This allows us to compare its effect with meta-reinforcement, which is activated on top of Hebbian reinforcement during the second stage, lasting T_2 loops, and acts only on Γ_{CG} . Finally, the system continues to evolve following a normal Hebbian dynamics, without meta-reinforcement, for T_3 loops.

We characterise the formation of memories (paths) by computing the path entropy $S_{\Sigma}(\Gamma)$, as this decreases with the emergence of preferred paths as shown in Fig. 3g). The choice of a specific meta-reinforced path Γ_{CG} allows us to characterise the interplay between reinforcement and meta-reinforcement by computing the distance, $d(\Gamma_T, \Gamma_{CG})$, between the path memorised at $T = T_1 + T_2 + T_3$ and Γ_{CG} . When reinforcement dominates, this distance will be large, as the two paths will have little in common. On the contrary, when meta-reinforcement dominates, the distance will be short, as the walker will follow the coarse-grained path Γ_{CG} . This protocol further allows us to test memory storing via meta-reinforcement alone. In this case we set all the weights to their initial values w_0 after $T_1 + T_2$ loops, thus erasing any Hebbian memory, and let the RW proceed for T_3 steps, checking whether path Γ_T is close to Γ_{CG} , meaning that the Hebbian dynamics in T_3 is able to retrieve a path stored through meta-reinforcement.

We investigate the following parameters: $p_{as} \in \{0.85, 0.95, 0.99\}$, $\tau \in \{4, 8, 16, 32, 64\}$, $c \in \{0, 0.25, 0.5, 1, 2, 4\}$. We set $T_1 = 100$, $T_2 = 1000$, and $T_3 = 19000$. These times allow to observe both reinforcement and meta-reinforcement effects, and their interplay. Their precise values do not affect the qualitative results obtained in this study, as shown in Supplementary material. T_3 in particular is sufficiently long to guarantee that the dynamics has reached a steady state for each combination of p_{as} , τ , and c . We perform 100 independent realisations for each combination of parameters p_{as} , τ , and c and average all measured quantities over them. Two example trajectories, one for a system showing memory ($p_{as} = 0.95$, $c = 2$, $\tau = 8$, $T_1 = 100$) and the other for a system that does not ($p_{as} = 0.95$, $c = 0$, $\tau = 8$, $T_1 = 100$), are

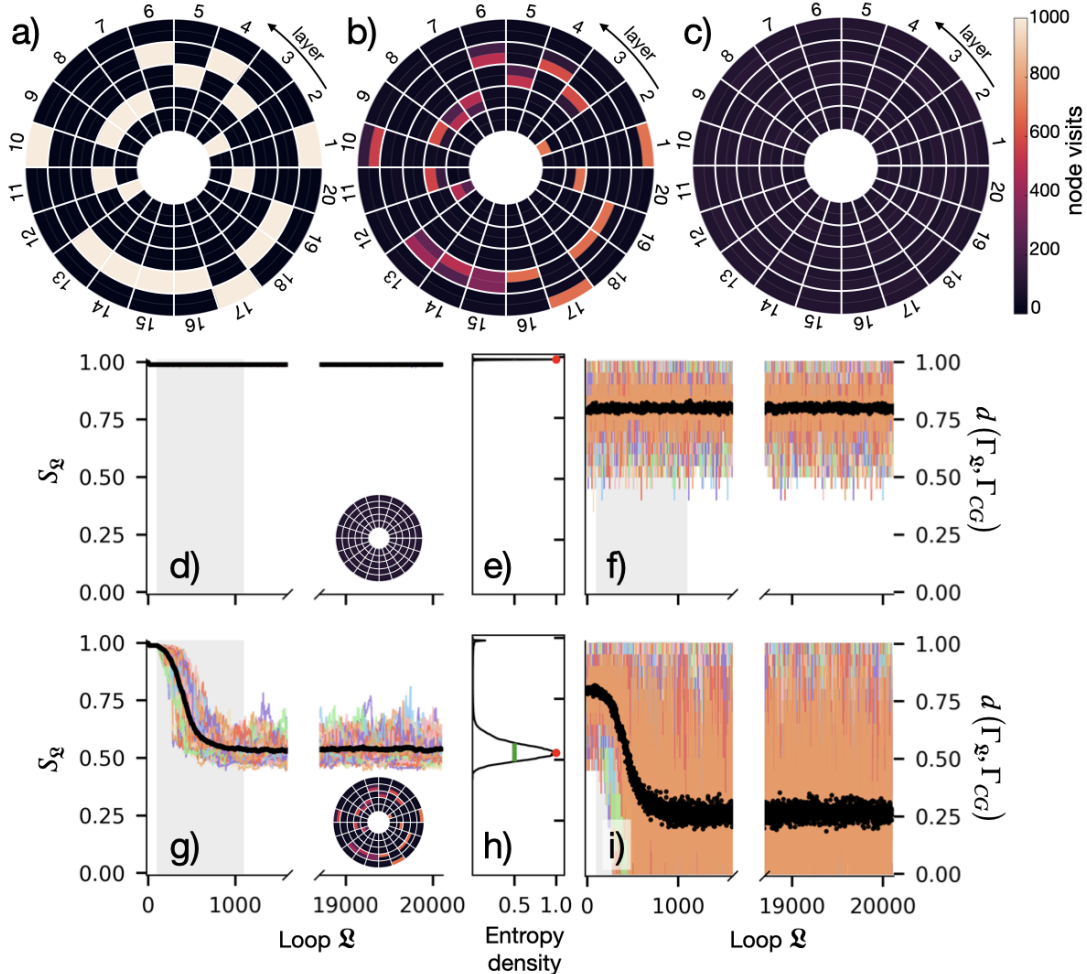


Figure 3. a) A random coarse-grained path Γ_{CG} to be memorised. b),c) Heatmaps of the visits (see colourbar on the right) of different nodes during the final 1000 loops for an individual realisation of b) a memorising process ($p_{as} = 0.95$, $c = 2$, $\tau = 8$, $T_1 = 100$) and c) a process that does not display memory ($p_{as} = 0.95$, $c = 0$, $\tau = 8$, $T_1 = 100$). White lines in a), b) and c) divide the network in layers and pairs of nodes, see Fig. 1. The time evolution of the normalised path entropy S_ℓ and distance from the target path $d(\Gamma_\ell, \Gamma_{CG})$ for the systems depicted in b) and c) are reported in panels g)-h) and d)-f) respectively. Coloured lines represent 100 independent realisations, black bullets their average at loop ℓ , and the grey shaded area the period T_2 of meta-reinforcement. The histograms of S_ℓ are reported in panels e) and h). Peaks are indicated in red, full-widths-at-half-maximum in green (visible in h)); for clarity the histogram is normalised to the highest peak.

reported in Fig. 3b) and c) respectively.

A. Memory formation

To observe whether a system is able to memorise, we compute its average path entropy and produce a histogram of the possible values. An illustrative example is reported in Fig. 3d+e) for $p_{as} = 0.95$, $c = 0$, $\tau = 8$, $T_1 = 100$ (no memory), g+h) for $p_{as} = 0.95$, $c = 4$, $\tau = 8$, $T_1 = 100$ (memorising). One can readily see that a memorising system shows a sharp decrease in entropy during the meta-reinforcement window T_2 (in grey), while the other one remains

constant after an initial small decrease due to reinforcement. Both systems reach a stable state in $\langle S_\ell \rangle$ (black bullets), also captured by the histograms. The memorising system shows two well-separated peaks: one at $S_\ell \gtrsim 0.98$, corresponding to the non-meta-reinforced process happening at the beginning of the simulation, and another at $S_\ell \sim 0.52$, indicating that the walker is traversing the meta-reinforced path Γ_{CG} . This fact is further captured by the average distance $\langle d(\Gamma_\ell, \Gamma_{CG}) \rangle$ reported in Fig. 3i) (black bullets).

The behaviour of path entropy and distance reported in Fig. 3 allows to identify a steady state in the dynamics. In all cases, this is reached well before the last 1000 loops in the run, and in general

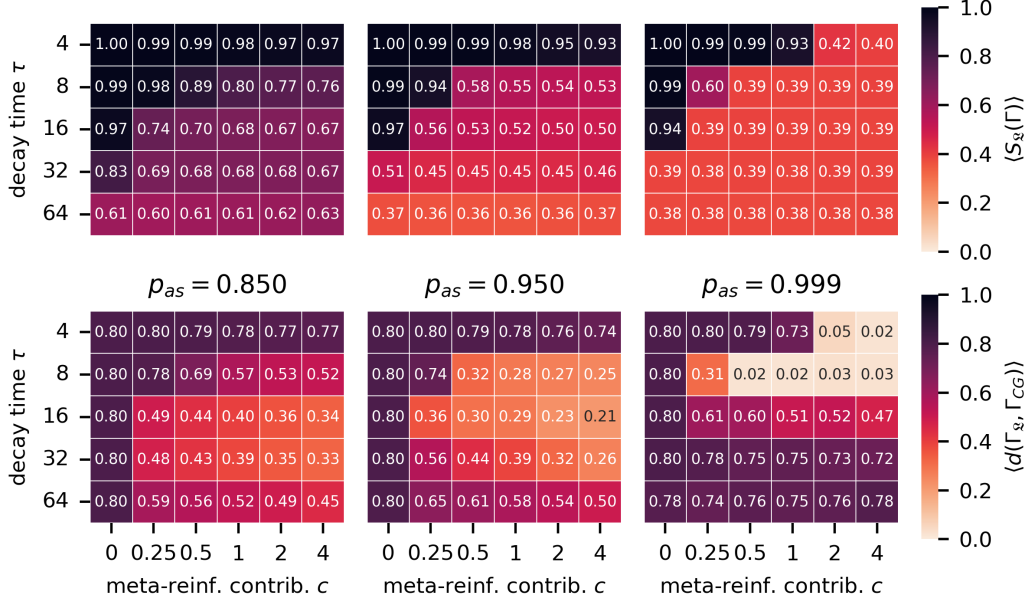


Figure 4. Heatmaps reporting stable states of the average path entropy $\langle S_{\mathcal{L}}(\Gamma) \rangle$ (top) and distance from the coarse-grained target path $\langle d(\Gamma_{\mathcal{L}}, \Gamma_{CG}) \rangle$ (bottom) as a function of decay time τ and meta-reinforcement contribution c for different values of maximal probability $p_{as} \in \{0.85, 0.95, 0.999\}$ and $T_1 = 100$. The columns corresponding to $c = 0$ in bottom heatmaps is not indicative of any system behaviour, as in absence of meta-reinforcement the distance from target path Γ_{CG} is uninformative.

shortly after $T_1 + T_2$.

We compare the memorisation ability of different systems by taking the time-averaged values, $\langle \cdot \rangle$, of $S_{\mathcal{L}}$ and $d(\Gamma_{\mathcal{L}}, \Gamma_{CG})$ over the last 1000 loops. The results, reported in Fig. 4, show several interesting effects of meta-reinforcement. First, meta-reinforcement can drive the formation of memory when reinforcement alone fails. This is evident from the behaviour of $\langle S_{\mathcal{L}} \rangle$ and $\langle d(\Gamma_{\mathcal{L}}, \Gamma_{CG}) \rangle$ for $\tau = 4, 8$, where one can observe that increasing c significantly lowers both the path entropy and the distance. For $p_{as} = 0.999$, $\tau = 8$ this change is particularly dramatic, with a $\approx 60\%$ decrease in entropy and an $\approx 97\%$ decrease in distance for $c \geq 1$: the system goes from a situation like the one reported in Fig. 3d+f) to one like that reported in Fig. 3g+i). Second, increasing both reinforcement (through the increase of τ) and meta-reinforcement leads to a process that memorises the wrong path, as can be seen from the heatmaps of $\langle d(\Gamma_{\mathcal{L}}, \Gamma_{CG}) \rangle$ in Fig. 4. Again, this is particularly evident for the case $p_{as} = 0.999$, where dynamics with $\tau = 64$, while having the lower values of $\langle S_{\mathcal{L}} \rangle$, display values of $\langle d(\Gamma_{\mathcal{L}}, \Gamma_{CG}) \rangle$ that are very close to those of a non-memorising case. On the contrary, the optimal combination is found for $\tau = 4, c = 4$ and $\tau = 8, c = 0.5, 1$. Varying T_1 does not change these results in any meaningful way, as shown in Fig. 8 in the Supplementary Material.

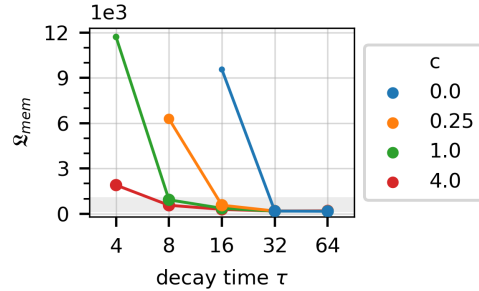


Figure 5. Average memorisation time \mathcal{L}_{mem} as functions of the decay times τ (in \log_2 -scale). Different curves correspond to different values of the meta-reinforcement contribution c (colours) for $p_{as} = 0.999$, $T_1 = 100$. Values are averaged over runs that did reach a state below S^* : bullet sizes reflect the amount of these runs, out of 100. The grey shaded area indicates the meta-reinforcement window from $\mathcal{L} = T_1$ to $\mathcal{L} = T_1 + T_2$.

The next question to consider is whether meta-reinforcement also affects the time needed to memorise a path (or a subset of paths). To define such a time, we leverage again the entropy histograms introduced in Fig. 3e+h). We define states of the system as the peaks in the histograms of S , characterised by a centre and a full-width-

at-half-maximum (FWHM). As can be seen from Fig. 3e+h), some states correspond to situations in which the system has no memory. For this reason, we define the “memorisation time” of a run, \mathfrak{L}_{mem} , as the number of loops necessary for the path entropy to reach the most populated state whose centre $S_c(\Gamma)$ is below a threshold value S^* . We consider $S^* = 0.74$ as this corresponds to the highest value of $\langle S_{\mathfrak{L}} \rangle$ for which $\langle d(\Gamma_{\mathfrak{L}}, \Gamma_{CG}) \rangle < 0.5$ in Fig. 4, i.e. the highest path entropy that still allows to recover at least half of the path that was meant to be memorised. The state is considered reached when $S_{\mathfrak{L}} < S_c + 1/2\text{FWHM}$. Since not all runs reach a state below S^* , in the following analysis we report the average values of \mathfrak{L}_{mem} computed only over runs in which memorisation did happen.

Fig. 5 depicts the results obtained as a function of the decay time τ for $c = 0, 0.25, 1, 4$ (colours), $\mathcal{P}_{as} = 0.999$. Bullet sizes reflect the amount of memorising runs, out of 100. The average number of loops to reach the memorising state, \mathfrak{L}_{mem} , depends on both τ and c . \mathfrak{L}_{mem} reaches a minimum for $\tau = 32$ and $\tau = 64$, with no significant difference as c changes: this memory is unrelated to meta-reinforcement, as highlighted also for Fig. 4. For $\tau < 32$, \mathfrak{L}_{mem} decreases with increasing c . Increasing τ reduces the impact of weight decay while increasing c reduces the time-scale of meta-reinforcement, both factors leading to a more rapid memorisation. Results for all values of p_{as} and c considered in this work are reported in Fig. 9 in the Supplementary Material, together with Table I detailing the number of memorising runs for each combination of parameters.

B. Memory retrieval

Finally, it is interesting to check whether a meta-reinforced path can be retrieved when all weights have been reset to zero, and the only difference between edges lies in the learning rates κ^ε , which are steeper for the meta-reinforced ones. This property is essential in systems, like the brain, that need to store new memories while maintaining access to old ones. To test this, we perform a series of runs in which at the end of the meta-reinforcement window $\mathfrak{L} = T_1 + T_2$, all variables s_t^ε are reset to zero, and all weights w_t^ε to w_0 . The RW then proceeds following the standard Hebbian dynamics described in Sec. II B for T_3 loops. Since this reset erases any and all short-term memory from the network, we do not consider the $c = 0$ case where meta-reinforcement is not present and any emerging memory is short-term memory. As before, we measure the path entropy $S_{\mathfrak{L}}$ and the distance from the stored path Γ_{CG} as function of \mathfrak{L} , averaged over 100 independent runs, and consider their

steady state values averaged over the last 1000 steps. The results, reported in Fig. 6, show that when the weights are reset, meta-reinforcement is still able to recall the correct path with a precision that is overall comparable to that obtained in Fig. 4 without the reset. Results for all values of p_{as} and c considered in this work are reported in Fig. 10 in the Supplementary Material, and show no qualitative change compared to what is reported here.

V. ASYMPTOTIC BEHAVIOUR OF META-REINFORCEMENT DYNAMICS

The interplay between meta-reinforcement and reinforcement can be understood more easily by considering the limit case in which a given edge in a group is always traversed, while all other edges in the same group are never chosen by the walker.

As described in section II, our model relies on a “hidden variable”, s , which influences the RW through the edge weight w . s grows linearly each time the walker traverses an edge, and decreases exponentially over time with decay time τ (in units of loops \mathfrak{L}). Under the assumption that an edge is always selected, these two contributions balance each other giving a limit value s_∞

$$s_\infty = \frac{1}{1 - e^{-\frac{1}{\tau}}}, \quad (12)$$

as can be found by imposing $s_{t+1} = s_t$ in Eq. 2. Expanding Eq. 12 around $\frac{1}{\tau} \sim 0$, one gets

$$s_\infty \simeq \tau + \frac{1}{2} + \frac{1}{12\tau} + o(\tau^{-2}) \quad (13)$$

so that for $\tau \gg 1$, $s_\infty \sim \tau + \frac{1}{2}$. Substituting Eq. 12 into Eq. 3, one gets an upper bound $w_{ub} < R$ for the maximum value reachable by the weights, $w_{ub} = \sigma(s_\infty)$. Using Eq. 13, this can be approximated as:

$$w_{ub} \simeq \frac{R}{1 + e^{-\kappa\tau - \frac{\kappa}{2} + \xi}}. \quad (14)$$

w_{ub} can thus be considered a logistic function of either κ or τ , whose upper bound is set by R . Due to the factor $\kappa\tau$, increasing τ leads to steeper functions of κ and vice versa, see Fig. 7.

It is important to note that the weight of any edge ε on the network reaches the maximum value w_{ub} as soon as ε is traversed τ consecutive times, and decreases again when the edge is not selected. For $p_{max} \sim 1$, however, consecutive traversal are probable and choosing a different path becomes more difficult, so that we can hope to get some insight on the results reported before for $p_{as} =$

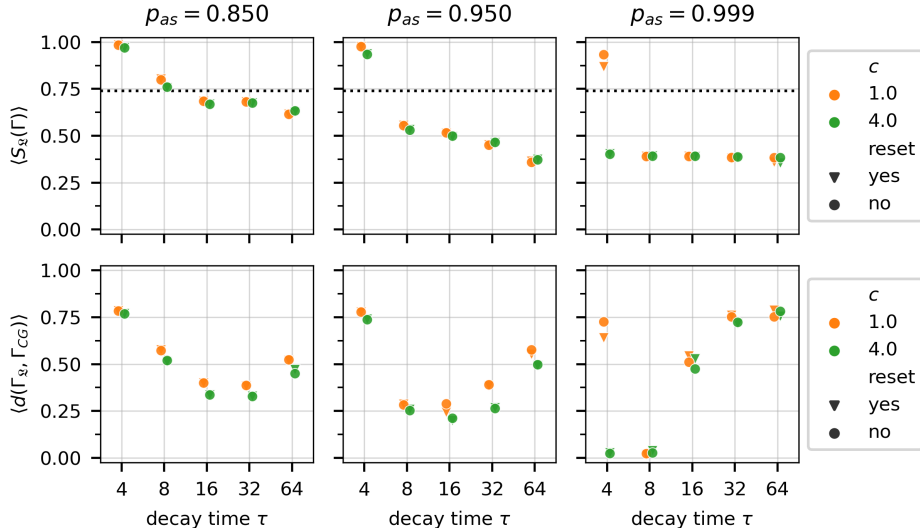


Figure 6. Memory retrieval analysis through path entropy (above) and distance (below) steady-state distributions as functions of the decay times τ (\log_2 scale), the meta-reinforcement coefficient c (colours) for $p_{as} = 0.999$. Symbols are slightly displaced along the x -axis to ease visualisation and comparison. Bullet shape reflects when the steady-state is computed: before (circular bullets) or after (triangular bullets) the reset. The dotted line in the top panels represents the $S^* = 0.74$ entropy threshold associated to memorisation.

0.999 by studying the behaviour of $w_{ub}(\kappa)$ at fixed τ , reported in Fig. 7 (bottom panel).

During our simulations, κ is increased for meta-reinforced edges, going from a value $\kappa_0 = 1$ to up to $\kappa = 2.25$ depending on the coefficient c . Fixing $\kappa = 1$ in Eq. 14, we get that the approximation to $w_{ub}(\kappa = 1)/R$ is equal to $\frac{1}{2}$ for $\tau^* = \xi - \frac{1}{2}$. Substituting the value of ξ used in this study, this gives $\tau^* = 8.6$. With this value of ξ we further get $w_{ub}(\kappa = 1)/R \geq 0.99$ for $\tau \geq 13$. Instead, for small values of τ $w_{ub}(\kappa = 1)/R \sim 0$, and $w_{ub}(\kappa = 2.25) < R$. We can thus identify three regimes of interplay between reinforcement and meta-reinforcement in the limit regime. For $\tau \gtrsim 14$, reinforcement dominates, as increasing κ leads to negligible increases in w_{ub} . For $\tau \lesssim 6$, meta-reinforcement can dominate, but only if κ is increased rapidly, i.e. for large values of c . For $\tau \sim 8$, instead, increasing κ considerably increases w_{ub} , leading to meta-reinforcement dominating over reinforcement also for relatively small values of c .

The limit regimes agree well with the behaviour observed in Sec. IV for the system with $p_{max} = 0.999$, both for memorisation and recall. In the first case, the results in Fig. 4 show that although the system reaches low entropy values for $\tau \geq 16$ the distance from the meta-reinforced path remains high, indicating that reinforcement is dominating. For $\tau = 4$, the meta-reinforced path begins to be recovered only for $c = 4$. $\tau = 8$ corresponds instead to a sweet-spot, minimising both

entropy and distance. A similar behaviour can be observed in Fig. 6, with $\tau = 8$ being the optimum and $\tau = 4$ competing with it only when $c = 4$. The same figures also show that this asymptotic argument loses strength when p_{max} is lowered. In that case, the interplay between reinforcement and meta-reinforcement should take into account also the average probability of choosing a reinforced edge, leading to a shift in the optimal value of τ . Intuitively, larger values of τ are needed to increase the probability of traversing the same edge s_∞ times. This analysis is left to a future work.

VI. CONCLUSION

In this manuscript we presented a simple model for a multi-level adaptive network whose connections follow a short-term Hebbian dynamics modulated by a long-term metaplastic mechanism. The latter has the effect of changing the “learning rate” with which different connections are reinforced. Our model describes phenomena in which a system of agents on a network adapt the topology of the latter to store information. This includes the case in which the agent is actually a walker exploring different locations. For simplicity, we implemented the dynamics as a biased random walk on a cyclic feed-forward network. While the model can be generalized to any network topology, this choice allowed us to easily compute the path en-

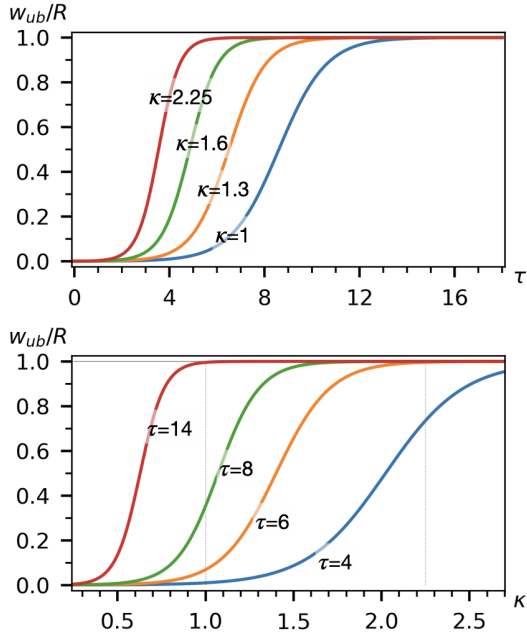


Figure 7. Normalised logistic functions w_{ub}/R . Top: w_{ub}/R as a function of τ for different values of κ^ε . Bottom: w_{ub}/R as a function of κ^ε for different values of τ . Dashed vertical lines represent the initial steepness $\kappa = 1$ and the maximal one achievable through meta-reinforcement $\kappa = 2.25$.

tropy and distance between paths, facilitating the analysis of the dynamics.

To the best of our knowledge, this is the first study investigating the dynamics of a system where plastic reinforcement is supported by a meta-plastic term changing the “learning rate” of selected connections.

By numerically exploring different parameters for the system, we have shown that there is a non-trivial interplay between plastic and meta-plastic reinforcements, depending on the decay time, τ , of the first and the rate, c , with which the second acts. We identified three regimes. In the first, for large values of τ , reinforcement dominates, and the long-term effect of meta-reinforcements has negligible influence. For small values of τ , the system starts showing memory only if the meta-reinforcement rate c is large. Interestingly, we also identified an intermediate regime in which even a small amount of meta-reinforcement can modulate memory formation. Above all, we showed that in the latter two regimes meta-reinforcement allows not only for the storing of a path, but also for its

retrieval when all weights have been reset to their initial value, i.e., when Hebbian memory has been erased. We rationalised our results by considering the limit case in which a single edge in a group is always selected, maximally reinforcing a weight. We show that the maximum value of the weight grows as a sigmoid whose steepness is controlled by τ and the meta-reinforcement term $\kappa(c)$, allowing one to recover the three regimes by comparing the values of τ and c .

The model presented in this work is inspired by brain dynamics and features but it is completely agnostic of the biological reality and suited to describe any two-scale memorisation process. Therefore, we believe our model to be applicable to any biological and social system and dynamics that can be mapped onto an adaptive network with multiple distinct memory contributions, particularly opinion diffusion, epidemics modelling and ecological networks.

ACKNOWLEDGEMENTS

We thank Dr. Beatrice Vignoli and Prof. Marco Canossa for helpful insights in the biological aspects of memory for the development of the model; Dr. Alessandro Ingrosso and Dr. Anže Božič for useful suggestions and discussions.

FUNDING

This research was supported by the European Research Council (ERC) under the European Union’s Horizon 2020 research and innovation program [grant agreement No. 788793, BACKUP].

AUTHOR CONTRIBUTIONS

LT, PB and LP conceived the work. LT, GZ, and PB devised a preliminary version of the model. GZ developed the model and the data analysis techniques with help from LT, PB and JM. GZ carried out simulations, cleaned and analysed data. All authors reviewed the results and contributed to their interpretation. GZ wrote the first draft of this manuscript. All authors contributed to and approved the final version of this manuscript.

[1] S. H. Strogatz, *Nature* **410**, 268 (2001), number: 6825 Publisher: Nature Publishing Group.

[2] S. Wuchty, E. Ravasz, and A.-L. Barabási, in *Complex Systems Science in Biomedicine*, edited by T. S. Deisboeck and J. Y. Kresh (Springer US,

- Boston, MA, 2006) pp. 165–181.
- [3] C. Castellano, S. Fortunato, and V. Loreto, *Reviews of Modern Physics* **81**, 591 (2009), publisher: American Physical Society.
- [4] K. Sneppen, S. Krishna, and S. Semsey, *Annual Review of Biophysics* **39**, 43 (2010).
- [5] V. Méndez, D. Campos, and F. Bartumeus, *Stochastic Foundations in Movement Ecology: Anomalous Diffusion, Front Propagation and Random Searches*, Springer Series in Synergetics (Springer, Berlin, Heidelberg, 2014).
- [6] R. Pastor-Satorras, C. Castellano, P. Van Mieghem, and A. Vespignani, *Reviews of Modern Physics* **87**, 925 (2015), publisher: American Physical Society.
- [7] J. Treur, *Network-Oriented Modeling: Addressing Complexity of Cognitive, Affective and Social Interactions*, Understanding Complex Systems (Springer International Publishing, Cham, 2016).
- [8] H. Dawid and D. Delli Gatti, in *Handbook of Computational Economics*, Vol. 4 (Elsevier, 2018) pp. 63–156.
- [9] B. Kozma and A. Barrat, *Physical Review E* **77**, 016102 (2008), publisher: American Physical Society.
- [10] A. Sirbu, V. Loreto, V. D. P. Servedio, and F. Tria, in *Participatory Sensing, Opinions and Collective Awareness*, edited by V. Loreto, M. Haklay, A. Hotho, V. D. Servedio, G. Stumme, J. Theunis, and F. Tria (Springer International Publishing, Cham, 2017) pp. 363–401.
- [11] F. Baumann, P. Lorenz-Spreen, I. M. Sokolov, and M. Starnini, *Physical Review Letters* **124**, 048301 (2020), publisher: American Physical Society.
- [12] T. Gross, C. J. D. D’Lima, and B. Blasius, *Physical Review Letters* **96**, 208701 (2006), publisher: American Physical Society.
- [13] G. Giordano, F. Blanchini, R. Bruno, P. Colaneri, A. Di Filippo, A. Di Matteo, and M. Colaneri, *Nature Medicine* **26**, 855 (2020), number: 6 Publisher: Nature Publishing Group.
- [14] J. Morand, S. Yip, Y. Velegrakis, G. Lattanzi, R. Potestio, and L. Tubiana, *Emergent circulation patterns from anonymized mobility data: Clustering Italy in the time of Covid* (2023), arXiv:2306.05302 [physics, q-bio].
- [15] M. C. González, C. A. Hidalgo, and A.-L. Barabási, *Nature* **453**, 779 (2008), number: 7196 Publisher: Nature Publishing Group.
- [16] M. Rosvall, A. V. Esquivel, A. Lancichinetti, J. D. West, and R. Lambiotte, *Nature Communications* **5**, 4630 (2014).
- [17] N. Gaumont, M. Panahi, and D. Chavalarias, *PLOS ONE* **13**, e0201879 (2018), publisher: Public Library of Science.
- [18] M. Cinelli, G. De Francisci Morales, A. Galeazzi, W. Quattrociochi, and M. Starnini, *Proceedings of the National Academy of Sciences* **118**, e2023301118 (2021), publisher: Proceedings of the National Academy of Sciences.
- [19] O. Vilck, D. Campos, V. Méndez, E. Lourie, R. Nathan, and M. Assaf, *Physical Review Letters* **128**, 148301 (2022).
- [20] J. J. Hopfield, *Proceedings of the National Academy of Sciences* **79**, 2554 (1982), publisher: Proceedings of the National Academy of Sciences.
- [21] J. J. Hopfield, *Proceedings of the National Academy of Sciences* **81**, 3088 (1984), publisher: Proceedings of the National Academy of Sciences.
- [22] D. C. Van Essen, S. M. Smith, D. M. Barch, T. E. Behrens, E. Yacoub, and K. Ugurbil, *Mapping the Connectome* **80**, 62 (2013).
- [23] W. James, in *The principles of psychology*, Vol. 1 (Henry Holt and Co, New York, NY, US, 1890) pp. 643–689.
- [24] N. Cowan, in *Progress in Brain Research*, Vol. 169, edited by W. S. Sossin, J.-C. Lacaille, V. F. Castellucci, and S. Belleville (Elsevier, 2008) pp. 323–338.
- [25] R. W. Semon, *Die Mneme als erhaltendes Prinzip im Wechsel des organischen Geschehens* (Engelmann, 1911).
- [26] D. O. Hebb, *The organization of behavior; a neuropsychological theory.*, The organization of behavior; a neuropsychological theory. (Wiley, Oxford, England, 1949).
- [27] S. A. Josselyn, S. Köhler, and P. W. Frankland, *Nature Reviews Neuroscience* **16**, 521 (2015).
- [28] S. A. Josselyn and S. Tonegawa, *Science* **367**, eaaw4325 (2020), publisher: American Association for the Advancement of Science.
- [29] E. Bienenstock, L. Cooper, and P. Munro, *The Journal of Neuroscience* **2**, 32 (1982).
- [30] P. Easton and P. E. Gordon, *Biological Cybernetics* **51**, 1 (1984).
- [31] W. Gerstner, R. Kempter, J. L. van Hemmen, and H. Wagner, *Nature* **383**, 76 (1996).
- [32] C. Clopath, L. Büsing, E. Vasilaki, and W. Gerstner, *Nature Neuroscience* **13**, 344 (2010).
- [33] M. McPherson, L. Smith-Lovin, and J. M. Cook, *Annual Review of Sociology* **27**, 415 (2001), eprint: <https://doi.org/10.1146/annurev.soc.27.1.415>.
- [34] J. Treur, *Network-Oriented Modeling for Adaptive Networks: Designing Higher-Order Adaptive Biological, Mental and Social Network Models*, Studies in Systems, Decision and Control, Vol. 251 (Springer International Publishing, Cham, 2020).
- [35] C. Hui, H. O. Minoarivelo, and P. Landi, *Mathematical Methods in the Applied Sciences* **41**, 8407 (2018).
- [36] J. Knebel, T. Krüger, M. F. Weber, and E. Frey, *Physical Review Letters* **110**, 168106 (2013), publisher: American Physical Society.
- [37] A. Baronchelli, L. Dall’Asta, A. Barrat, and V. Loreto, *Physical Review E* **76**, 051102 (2007), publisher: American Physical Society.
- [38] J. T. Matamalas, M. De Domenico, and A. Arenas, *Journal of The Royal Society Interface* **13**, 20160203 (2016), publisher: Royal Society.
- [39] A. Araque, V. Parpura, R. P. Sanzgiri, and P. G. Haydon, *Trends in Neurosciences* **22**, 208 (1999).
- [40] E. A. Newman, *Trends in Neurosciences* **26**, 536 (2003).

- [41] M. De Pittà, V. Volman, H. Berry, V. Parpura, A. Volterra, and E. Ben-Jacob, *Frontiers in Computational Neuroscience* **6**, 98 (2012).
- [42] M. De Pittà, N. Brunel, and A. Volterra, *Dynamic and metabolic astrocyte-neuron interactions in healthy and diseased brain* **323**, 43 (2016).
- [43] A. Araque, G. Carmignoto, P. G. Haydon, S. H. R. Oliet, R. Robitaille, and A. Volterra, *Neuron* **81**, 728 (2014).
- [44] M. De Domenico, A. Solé-Ribalta, E. Cozzo, M. Kivela, Y. Moreno, M. A. Porter, S. Gómez, and A. Arenas, *Physical Review X* **3**, 041022 (2013).
- [45] M. E. Dickison, M. Magnani, and L. Rossi, *Multilayer Social Networks* (Cambridge University Press, 2016).
- [46] S. Pilosof, M. A. Porter, M. Pascual, and S. Kéfi, *Nature Ecology & Evolution* **1**, 1 (2017), number: 4 Publisher: Nature Publishing Group.
- [47] M. De Domenico, *Nature Physics* **19**, 1247 (2023).
- [48] Y. Mukerija, J. Treur, and S. Hendrikse, *Cognitive Systems Research* **84**, 101187 (2024).
- [49] S. Fusi, P. J. Drew, and L. Abbott, *Neuron* **45**, 599 (2005).
- [50] P. Yger and M. Gilson, *Frontiers in Computational Neuroscience* **9**, 10.3389/fncom.2015.00138 (2015).
- [51] G. M. Schütz and S. Trimper, *Physical Review E* **70**, 045101 (2004), publisher: American Physical Society.
- [52] M. Holmes and A. Sakai, *Stochastic Processes and their Applications* **117**, 1519 (2007).
- [53] E. Agliari, R. Burioni, and G. Uguzzoni, *New Journal of Physics* **14**, 063027 (2012), publisher: IOP Publishing.
- [54] J. C. Cressoni, G. M. Viswanathan, A. S. Ferreira, and M. A. A. da Silva, *Physical Review E* **86**, 042101 (2012).
- [55] A. Gut and U. Stadtmüller, *Statistics & Probability Letters* **189**, 109598 (2022).
- [56] M. D. Donsker and S. R. S. Varadhan, *Communications on Pure and Applied Mathematics* **32**, 721 (1979), publisher: John Wiley & Sons, Ltd.
- [57] Vlada Limic and Pierre Tarrès, *The Annals of Probability* **35**, 1783 (2007).
- [58] D. Campos, F. Bartumeus, and V. Méndez, *Physical Review E* **96**, 032111 (2017).
- [59] D. Erhard, T. Franco, and G. Reis, *Journal of Statistical Physics* **190**, 18 (2022).
- [60] B. Davis, *Probability Theory and Related Fields* **84**, 203 (1990).
- [61] R. Gesztelyi, J. Zsuga, A. Kemeny-Beke, B. Varga, B. Juhasz, and A. Tosaki, *Archive for History of Exact Sciences* **66**, 427 (2012).
- [62] E. T. Jaynes, *Annual Review of Physical Chemistry* **31**, 579 (1980), publisher: Annual Reviews.
- [63] S. Pressé, K. Ghosh, J. Lee, and K. A. Dill, *Reviews of Modern Physics* **85**, 1115 (2013), publisher: American Physical Society.

Appendix: Supplementary Material

1. Derivation of path entropy for a CFFN

The following derivation is almost analogous to the one detailed by Pressé *et al.* [63]: the network we consider is not only feed-forward but also cyclic, which allows us to measure time in units of loops \mathcal{L} around the network.

Mathematically, the generic definition of entropy in information theory is

$$S(X) = - \sum_{x \in \mathcal{X}} \mathcal{P}(x) \ln(\mathcal{P}(x)) \quad (\text{A.1})$$

where X is a discrete random variable assuming values $x \in \mathcal{X}$ alphabet with probability $\mathcal{P}(x)$. Similarly, we can define the path entropy for a RW on a network G as

$$S(RW) = - \sum_{\{\Gamma\}} \mathcal{P}(\Gamma) \ln(\mathcal{P}(\Gamma)) \quad (\text{A.2})$$

where the generic path $\Gamma = \{x_{t_i}, \dots, x_{t_j}\}$ is a set of the nodes visited or edges traversed by the random walker between times t_i and t_j ; $\{\Gamma\}$ is the set of all possible paths with that same time duration, each being walked with probability $\mathcal{P}(\Gamma)$. In principle, this is the equation to use for RW dynamics on a generic network; however, we can take advantage of our network being a CFFN to

simplify the expression. First of all, we can take advantage of the definition of time-step we gave above and consider Γ as the path during one loop of RW: $\Gamma = \Gamma_{\mathcal{L}}$. Moreover, we can take advantage of the formalism of transition matrices. A transition matrix $T_t^{j \leftarrow i}$ is the matrix of probabilities of going from any node i to any node j in the network at time-step t : it evolves with the RW. For the CFFN it reduces to $T_{\mathcal{L}}^{(\ell, j) \leftarrow (\ell-1, i)}$ where time is measured in units of loops on the network and notation (ℓ, j) means that node j belongs to the ℓ^{th} layer. Finally, as detailed in the main text, the closed topology of a CFFN means each loop starts in the node where the previous one ends: write $n_{\mathcal{L}}^{\ell=0} \equiv n_{\mathcal{L}-1}^{\ell=L}$ as the node of the layer L visited by the walker in the previous loop $\mathcal{L} - 1$. From here, $\mathcal{P}(n_{\mathcal{L}}^{\ell=0})$ is the probability for the previous loop to end in node $n_{\mathcal{L}}^{\ell=0}$ and $T_{\mathcal{L}}^{\ell=1 \leftarrow \ell-1=0}$ is the transition matrix from the last layer of the previous loop to the first of the current loop. This is analogous to a Kronecker delta term $\delta_{\ell=0, \ell=L}$ that closes the network, i.e. it ensures the L^{th} layer of a loop becomes the 0^{th} of the following one. Therefore, given $\Gamma_{\mathcal{L}} = \{x^{\ell}\}$ a sequence of L steps of the RW we have:

$$\mathcal{P}(\Gamma_{\mathcal{L}}) = \prod_{\ell=1}^L p(x_{\mathcal{L}}^{\ell=0}) T_{\mathcal{L}}^{x^{\ell} \leftarrow x^{\ell-1}}. \quad (\text{A.3})$$

Plugging Eq. (A.3) into the logarithm we get

$$\ln(p(\Gamma_{\mathcal{L}})) = \ln\left(\prod_{\ell=1}^L p(x_{\mathcal{L}}^{\ell=0}) T_{\mathcal{L}}^{x^{\ell} \leftarrow x^{\ell-1}}\right) = \ln(p(x_{\mathcal{L}}^{\ell=0})) + \sum_{\ell=1}^L \ln\left(T_{\mathcal{L}}^{x^{\ell} \leftarrow x^{\ell-1}}\right). \quad (\text{A.4})$$

Finally, combining Eq. (A.3) and Eq. (A.4) in

Eq. (A.2) we get

$$S_{\mathcal{L}}(RW) = - \sum_{\{\Gamma_{\mathcal{L}}\}} \prod_{\ell=1}^L p(x_{\mathcal{L}}^{\ell=0}) T_{\mathcal{L}}^{x^{\ell} \leftarrow x^{\ell-1}} \left[\ln(p(x_{\mathcal{L}}^{\ell=0})) + \sum_{\ell=1}^L \ln\left(T_{\mathcal{L}}^{x^{\ell} \leftarrow x^{\ell-1}}\right) \right] \quad (\text{A.5})$$

which is the same equation as Eq. (9) and represents the path entropy at loops \mathcal{L} for a RW process on a CFFN.

2. Further results

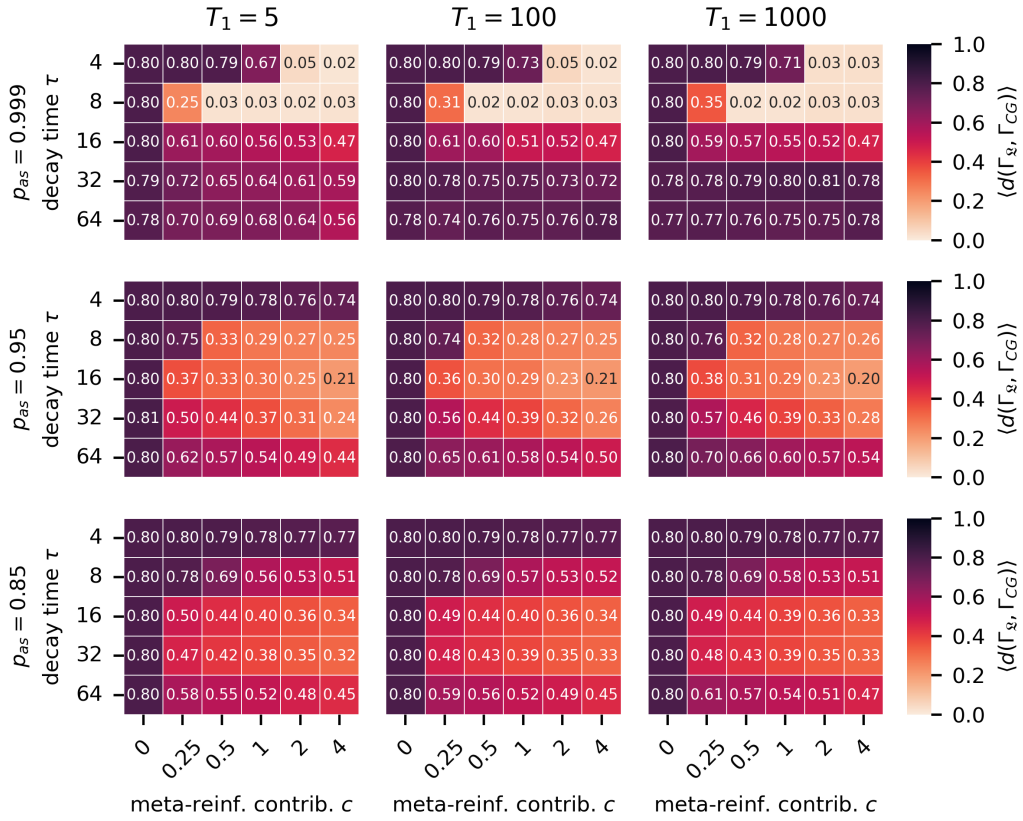


Figure 8. Path distance heatmaps for all values of T_1 . Heatmaps reporting stable states of the average distance from the coarse-grained target path $\langle d(\Gamma_{\Sigma}, \Gamma_{CG}) \rangle$ as a function of decay time τ and meta-reinforcement contribution c for different values of maximal probability $p_{as} \in \{0.85, 0.95, 0.999\}$. The columns corresponding to $c = 0$ in bottom heatmaps is not indicative of any system behaviour, as in absence of meta-reinforcement the distance from target path Γ_{CG} is uninformative. Heatmaps reporting stable states of the average path entropy $\langle S_{\Sigma}(\Gamma) \rangle$ (top) and distance from the coarse-grained target path $\langle d(\Gamma_{\Sigma}, \Gamma_{CG}) \rangle$ (bottom) as a function of decay time τ and meta-reinforcement contribution c for different values of maximal probability $p_{as} \in \{0.85, 0.95, 0.999\}$. The columns corresponding to $c = 0$ in bottom heatmaps is not indicative of any system behaviour, as in absence of meta-reinforcement the distance from target path Γ_{CG} is uninformative. Average path entropy $\langle S_{\Sigma}(\Gamma) \rangle$ stable states are not reported as parameter T_1 has little to no influence over them.

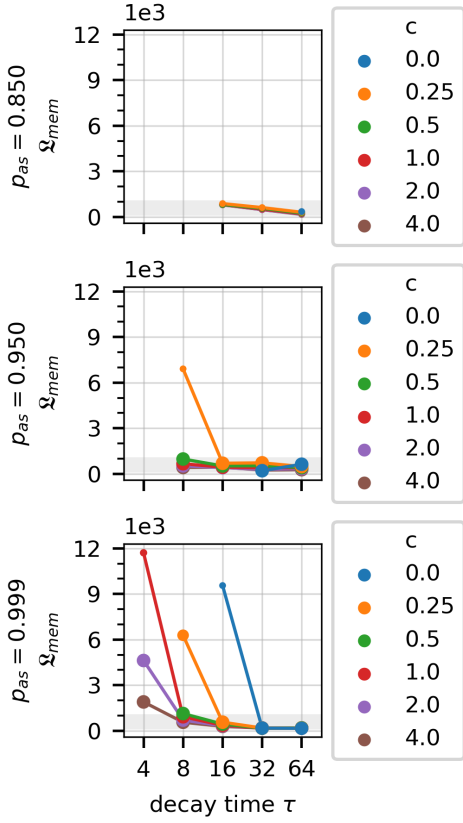


Figure 9. Average memorisation time \mathfrak{L}_{mem} as functions of the decay times τ (in \log_2 -scale) for different values of maximal probability $p_{as} \in \{0.85, 0.95, 0.999\}$ and $T_1 = 100$. Different curves correspond to different values of the meta-reinforcement contribution c (colours). Values are averaged over runs that did reach a state below S^* : bullet sizes reflect the amount of these runs, out of 100. The grey shaded area indicates the meta-reinforcement window from $\mathfrak{L} = T_1$ to $\mathfrak{L} = T_1 + T_2$.

		# of memorising runs (out of 100)				
p_{as}	c	τ				
		4	8	16	32	64
0.85	0					100
	0.25			100	100	100
	0.5			100	100	100
	1			100	100	100
	2			100	100	100
	4			100	100	100
0.95	0				100	100
	0.25		24	100	100	100
	0.5		100	100	100	100
	1		100	100	100	100
	2		100	100	100	100
	4		100	100	100	100
0.999	0			4	100	97
	0.25		65	100	99	96
	0.5		100	100	99	97
	1	9	100	100	97	97
	2	99	100	99	99	96
	4	100	100	100	98	98

Table I. Number of memorising runs, out of 100 identical ones, for different combinations of decay τ , meta-reinforcement c^k and maximal probability \mathcal{P}_{max} for $T_1 = 100$. Only non-null cases are reported. Memorisation is identified through path entropy states analysis.

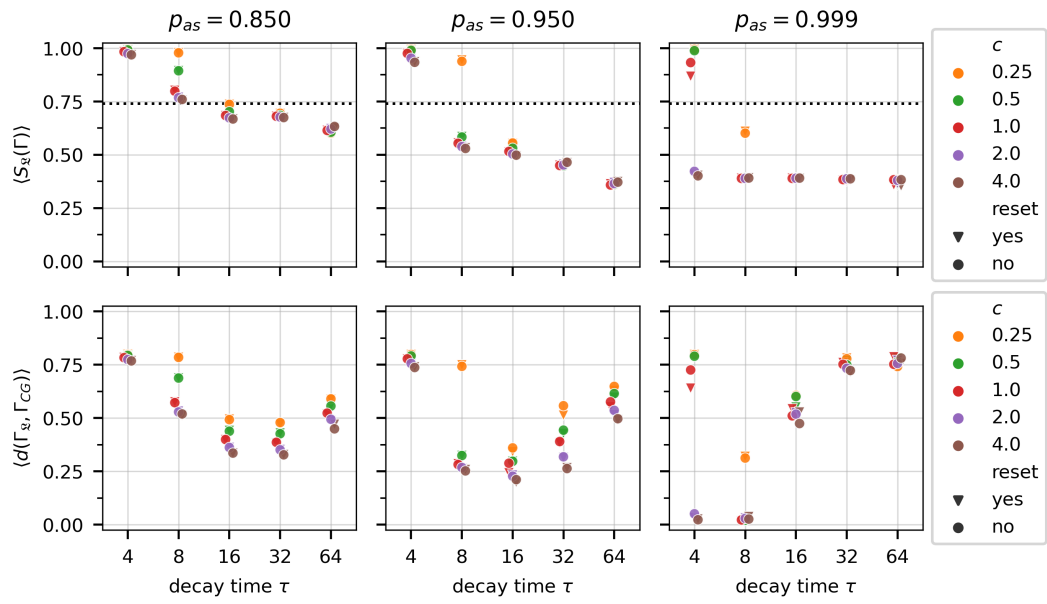


Figure 10. Recall analysis through path entropy (above) and distance (below) steady-state distributions as functions of the decay times τ (\log_2 scale), the meta-reinforcement coefficient c (colours) for different values of maximal probability $p_{as} \in \{0.85, 0.95, 0.999\}$ and $T_1 = 100$. Symbols are slightly displaced along the x -axis to ease visualisation and comparison. Bullet shape reflects when the steady-state is computed: before (circular bullets) or after (triangular bullets) the reset. The dotted line in the top panels represents the threshold $S^* = 0.74$ associated to memorisation.